Metal-metal interactions in dinuclear ruthenium complexes containing bridging 4,5-di(2-pyridyl)imidazolates and related ligands

Jonathan W. Slater,[a] Deanna M. D'Alessandro,[b] F. Richard Keene[b] and Peter J. Steel*[a]

[a] *Department of Chemistry, University of Canterbury, Christchurch, New Zealand*
Email: peter.steel@canterbury.ac.nz
[b] *School of Pharmacy & Molecular Sciences, James Cook University, Townsville, Queensland 4811, Australia*

Paper Ref.: B514976M

ELECTRONIC SUPPLEMENTARY INFORMATION

Table S1 UV/Vis/NIR spectral data of the reduced absorption spectra (ε/ν *vs.* ν) for $\mathbf{3}^{n+}$ and $\mathbf{4}^{n+}$ in 0.1 M $[(n\text{-}C_4H_9)_4N]PF_6/CH_3CN$ at -35°C. The NIR spectral data are indicated in bold type.[a]

Complex	n+	**3**	**4**
		$\nu_{max} \pm 10$ /cm^{-1} $\{(\varepsilon/\nu)_{max} \pm 0.0001$ /M^{-1}cm$^{-1}\}$	$\nu_{max} \pm 10$ /cm^{-1} $\{(\varepsilon/\nu)_{max} \pm 0.0001$ /M^{-1}cm$^{-1}\}$
meso	4	*sh* 17830 (0.3011) 20160 (0.6828) 24590 (0.8858)	*sh* 16702 (0.3970) 19000 (0.9673) 23510 (0.8643)
	5	**6590 (1.5218)** 15880 (0.2575) 18870 (0.4582) 24920 (0.4084)	**5625 (1.4908)** 14380 (0.1880) 17810 (0.5303) 23543 (0.3379)
	6	~12359 (0.0519) 18771 (0.1312) 22671 (0.2185)	
rac	4	*sh* 17892 (0.3743) 20190 (0.7951) 24620 (1.0359)	*sh* 16690 (0.3992) 18920 (0.9629) 23570 (0.9117)
	5	**6460 (1.2737)** 15895 (0.1883) 18840 (0.3703) 24910 (0.3522)	**5628 (0.8994)** 14410 (0.2326) 18370 (0.5161) 23930 (0.4854)

[a] ***meso*4**$^{6+}$, ***rac*3**$^{6+}$ and ***rac*4**$^{6+}$ not measured.

Table S2 UV/Vis/NIR spectral data of the reduced absorption spectra (ε/ν *vs.* ν) for $\mathbf{9}^{n+}$ in 0.1 M [(*n*-$C_4H_9)_4N]PF_6/CH_3CN$ and 0.02 M [(*n*-$C_4H_9)_4N]\{B(C_6F_5)_4\}/CH_3CN$ at -35°C. The NIR spectral data are indicated in bold type.[a]

Complex	*n*+	PF_6^- $\nu_{max} \pm 10$ /cm^{-1} $\{(\varepsilon/\nu)_{max} \pm 0.0001$ /M^{-1}cm$^{-1}\}$	$\{B(C_6F_5)_4\}^-$ $\nu_{max} \pm 10$ /cm^{-1} $\{(\varepsilon/\nu)_{max} \pm 0.0001$ /M^{-1}cm$^{-1}\}$
9a^{n+} ***meso***	3	21305 (1.3060)	21290 (1.3189)
		22480 (1.2337)	22354 (1.2414)
		27935 (0.9329)	27920 (0.9383)
	4	**4560 (1.2061)**	**4105 (0.9119)**
		9806 (0.3258)	9110 (0.2793)
		10700 (0.2668)	9990 (0.2204)
		22340 (0.8190)	22190 (0.6665)
		28370 (0.9067)	27725 (0.7955)
	5	18965 (0.3752)	19385 (0.2488)
		27768 (1.0277)	26885 (0.8709)
		28865 (1.1227)	28100 (0.9049)
9a^{n+} ***rac***	3	21070 (1.3192)	21065 (1.3255)
		22650 (1.2322)	22520 (1.2433)
		28010 (1.0122)	28025 (0.9951)
	4	**4474 (1.4816)**	**4117 (0.9668)**
		9818 (0.4286)	9116 (0.2658)
		10730 (0.3762)	10062 (0.2163)
		22295 (1.0266)	22205 (0.6515)
		28445 (1.1114)	27845 (0.8682)
	5	18890 (0.4771)	19430 (0.2157)
		27600 (1.2592)	26930 (0.9165)
		28580 (1.3522)	28130 (0.9638)

Table S3 NIR spectral data of the reduced absorption spectra (ε/ν *vs.* ν) for $\mathbf{3}^{5+}$ and $\mathbf{4}^{5+}$ in 0.1 M [(*n*-$C_4H_9)_4N]PF_6/CH_3CN$ at -35°C. For the dinuclear species, the parameters for the overall NIR band envelopes are shown in bold type: details of the deconvoluted bands are in normal type.

Complex	Component	ν_{max} ± 10 /cm^{-1}	$(\varepsilon/\nu)_{max}$ ± 0.0001 /M^{-1}	$\Delta\nu_{1/2}$ ± 20 /cm^{-1}	$\Delta\nu_{1/2}^{o}$ /cm^{-1}	M_0 /M^{-1}	H_{ab} /cm^{-1}
3*meso*$^{5+}$		**6590**	**1.5218**	**1470**	**3480**	**3211**	**3295**
	1	5140	0.3339	1330		472.1	
	2	6570	1.3959	1210		1802	2570
	3	7686	0.3742	1620		645.7	
3*rac*$^{5+}$		**6460**	**1.2737**	**1492**	**3440**	**2650**	**3230**
		3782	0.2670	1950		350.9	
	1	5020	0.1574	1050		175.9	
	2	6438	0.9936	1267		1340	2510
	3	7650	0.2676	1564		445.7	
4*meso*$^{5+}$		**5625**	**1.4908**	**1346**	**3210**	**2538**	**2813**
	1	4425	0.2682	850.4		241.5	
	2	5600	1.4058	1023		1530	2800
	3	6460	0.4536	1016		490.7	
		7175	0.1540	1405		230.4	
4*rac*$^{5+}$		**5628**	**0.8995**	**1516**	**3215**	**1656**	**2814**
	1	4400	0.1552	790		130.1	
	2	5600	0.8453	1093		984.3	2800
	3	6515	0.3023	1050		338.5	
		7260	0.1076	1543		176.8	

Table S4 NIR spectral data of the reduced absorption spectra (ε/ν *vs.* ν) for $\mathbf{9}^{4+}$ in 0.1 M [(*n*-$C_4H_9)_4N]PF_6/CH_3CN$ and 0.02 M [(*n*-$C_4H_9)_4N]\{B(C_6F_5)_4\}/CH_3CN$ at -35°C. The parameters for the overall NIR band envelopes are shown in bold type and details of the deconvoluted bands are in normal type.[a]

Electrolyte	Complex	Component	ν_{max} ± 10 /cm^{-1}	$(\varepsilon/\nu)_{max}$ ± 0.0001 /M^{-1}	$\Delta\nu_{1/2}$ ± 20 /cm^{-1}	$\Delta\nu_{1/2}^{o}$ /cm^{-1}	M_0[c] /M^{-1}	H_{ab} /cm^{-1}
PF_6^-	**9*rac*$^{4+}$**		**4475**	**1.4816**	**1112**[b]	**2866**		**2238**
		2	4450	1.4006	1947		2693	
		3	6340	0.2124	1570		355	
		4	9678	0.2765	1370		404	
		5	10950	0.2003	1540		328	
		6	12310	0.08094	2005		172	
	9*meso*$^{4+}$		**4560**	**1.2061**	**1029**[b]	**2893**		**2280**
		2	4302	1.2301	2380		2663	
		3	6582	0.1270	1984		268	
		4	9797	0.2982	1580		500	
		5	11117	0.1378	1204		176	
		6	12185	0.0873	2032		188	
$\{B(C_6F_5)_4\}^-$	**9*rac*$^{4+}$**		**4120**	**0.9668**	**1148**[b]	**2750**		**2060**
		2	3980	0.9351	2230		1625	
		3	6058	0.1318	2040		285	
		4	9140	0.2377	1640		415	
		5	10410	0.08727	1152		107	
		6	11347	0.07440	1990		157	
	9*meso*$^{4+}$		**4105**	**0.9119**	**1160**[b]	**2745**		**2053**
		2	3960	0.9151	2355		1683	
		3	6197	0.1287	1816		248	
		4	9128	0.2551	1636		444	
		5	10430	0.08557	1130		103	
		6	11293	0.07602	2090		170	

[a] The first component was obscured at the detector limit and an accurate determination of the parameters was precluded.

[b] Bandwidth for the high-energy side of the IVCT manifold. The lower energy side was obscured at the detector limit.

[c] The M_0 for the full band manifold could not be measured reliably.

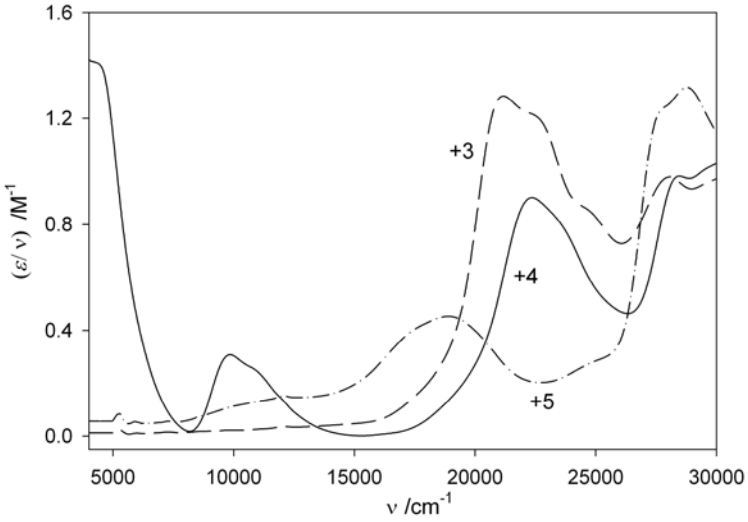

Figure S1 Overlay of the spectra for **9*rac***$^{n+}$ {n = 3, 4, 5} in 0.1 M [(n-C_4H_9)$_4$N]PF_6/CH_3CN at -35°C.

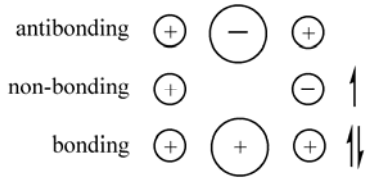

Figure S2 Qualitative molecular orbital diagram for the dinuclear [{Ru(bpy)$_2$}$_2$(μ-BL)]$^{5+}$ systems showing the bonding, non-bonding and antibonding molecular orbitals. The IVCT corresponds to a bonding → non-bonding transition.